

Article

Manufacturing of Continuous Carbon Fiber Reinforced Aluminum by Spark Plasma Sintering

Miguel Jiménez *, Felix Ott, Frank Kern and Rainer Gadow

Institute for Manufacturing Technologies of Ceramic Components and Composites, University Stuttgart, Allmandring 7b, D-70569 Stuttgart, Germany; felix.ott@ifkb.uni-stuttgart.de (F.O.); frank.kern@ifkb.uni-stuttgart.de (F.K.); rainer.gadow@ifkb.uni-stuttgart.de (R.G.)

* Correspondence: miguel.jimenez@ifkb.uni-stuttgart.de; Tel.: +49-711-685-68227

Received: 8 June 2020; Accepted: 29 June 2020; Published: 30 June 2020



Abstract: In the field of metal matrix composites (MMC), spark plasma sintering (SPS) technique has been used so far for the manufacture of particle, whisker and short-fiber reinforced alloys. In this work, SPS technique is employed for the first time to produce continuous fiber reinforced light metals. For this purpose, metal matrix composite prepregs with aluminum as a surface coating on carbon fiber textiles are manufactured by twin arc wire spraying and subsequently consolidated by SPS in the semi-solid temperature range of the alloy. Shear thinning rheological behavior of the metal alloy at temperatures between solidus and liquidus enables the infiltration of fiber rovings under reduced forming loads. SPS offered a better controlled and more efficient heat transfer in the green body and faster consolidation cycles in comparison with alternative densification methods. Fully densified samples with no porosity proved the suitability of SPS for densification of MMC with a remarkable stiffness increase in comparison with samples densified by thixoforging, an alternative consolidation method. However, the pulse activated sintering process leads to a quite strong fiber/matrix adhesion with evidence of aluminum carbide formation.

Keywords: metal matrix composites (MMC); aluminum matrix composites (AMC); spark plasma sintering (SPS); carbon fiber; semi-solid forming

1. Introduction

Aluminum has become the preferred structural material for a myriad of applications in the fields of ground transportation and aeronautics because of its low density in comparison with carbon steel. Nevertheless, specific demands of certain components require the use of alternative lightweight materials with higher stiffness and targeted thermo-physical properties. Due to this reason, metal matrix composites (MMC) have been in focus of research over the last 50 years. By adequate selection of reinforcing phase and composite architecture, different objectives can be achieved by the substitution of conventional materials by MMC components such as, Young's modulus increase, reduction of thermal elongation and creep resistance increase [1]. For niche applications in sectors of low pricing pressure, such as aerospace, different material solutions based on ceramic fiber (SiC, Al₂O₃) reinforced light metals have been developed since the 1980s [2]. However, for the establishment of fiber reinforced light metals in application fields with tough cost targets, as ground transportation or mechanical engineering, low-priced raw materials and economically viable manufacturing processes are required.

The search for synergies between outstanding mechanical properties of low-priced polyacrylonitrile-based carbon fibers and the low density of aluminum has attracted wide attention from academia and industry. However, the chemical compatibility of the matrix and reinforcing phase of this material system is still today an unresolved technical hurdle. The uncontrolled growth of aluminum carbide crystals, which are formed at the C_f/Al interface during high-temperature exposures,

has been proven to impair mechanical properties of such composites. Several publications have contributed to a better understanding of growth mechanisms and implications of interfacial Al_4C_3 nanocrystals for the micro- and macro mechanical properties of C_f/Al [3–7]. According to the published literature about this topic, the compatibility of C_f/Al interface can be optimized by different strategies:

- Deposition of thin ceramic or metallic interlayers at the interface [8–10];
- Functionalization of fiber surface; targeted selection of carbon fibers with suitable surface topography [11];
- Selection of aluminum alloys with certain levels of alloying elements, which contribute to inhibition of Al_4C_3 growth [12,13];
- Optimization of manufacturing parameters for the reduction of thermal exposure.

The last two strategies are especially interesting from the point of view of cost effectiveness, because their application is linked with no further manufacturing steps. For their implementation, a wide knowledge about the most suitable manufacturing parameters, concerning interfacial properties optimization for different aluminum alloys, is necessary. However, and according to the state of the art previous to this publication, this study has not been conducted so far.

Considering published literature, carbide growth and therefore interfacial properties are very sensitive to minor gradients of temperature during shaping and post-treatment [6]. Therefore, it is necessary to operate with a very accurate control of processing parameters for a decent study on optimization of time–temperature progression.

Spark plasma sintering (SPS), which has been investigated in the recent years not only for the manufacturing of high-performance ceramics but also for consolidation of particle [14,15], carbon nanotube [16] and short fiber reinforced light metals [17,18], is a technically feasible tool to perform this task. The aim of this work is conducting for first time a feasibility study on the SPS consolidation of continuously reinforced aluminum matrix composites. In order to compare the obtained results of samples densified by SPS with an alternative method, MMC reference samples are manufactured by thixoforging with a hydraulic press from the same raw materials.

2. Materials and Methods

For the study on SPS consolidation of continuous fiber reinforced aluminum following raw materials were employed:

- Reinforcement: Carbon fiber woven fabrics in plain weave binding with an areal weight of 160 g/m^2 from HT 200 tex 3k carbon rovings
- Matrix: Wires of 1.6 mm diameter supplied by Drahtwerk Elisental (Neuenrade, Germany) of aluminum alloys AlSi1MgMn, AlSi5, AlSi7Mg, and AlSi10Mg. Chemical compositions of every alloy are shown in Table 1.

Table 1. Chemical composition of aluminum alloys according to manufacturer specifications.

Sample	Si (%)	Fe (%)	Cu (%)	Mn (%)	Mg (%)	Zn (%)	Ti (%)	Be (%)	Al (%)
AlSi1MgMn	1.03	0.31	0.08	0.47	1.09	0.01	0.01	n.s.	Rest
AlSi5	5.10	0.11	0.01	0.00	0.01	0.00	0.01	0.001	Rest
AlSi7Mg	6.90	0.11	0.001	0.001	0.67	0.001	0.09	0.001	Rest
AlSi10Mg	9.30	0.16	0.00	0.00	0.26	0.00	0.02	0.001	Rest

The manufacturing process chain followed in this study is summarized in Figure 1. Woven fabrics were initially cut into sheets, which were coated with the metallic matrix by means of thermal spraying. The resulting MMC prepregs were consolidated to C_f/Al samples by two different methods: SPS and thixoforging.

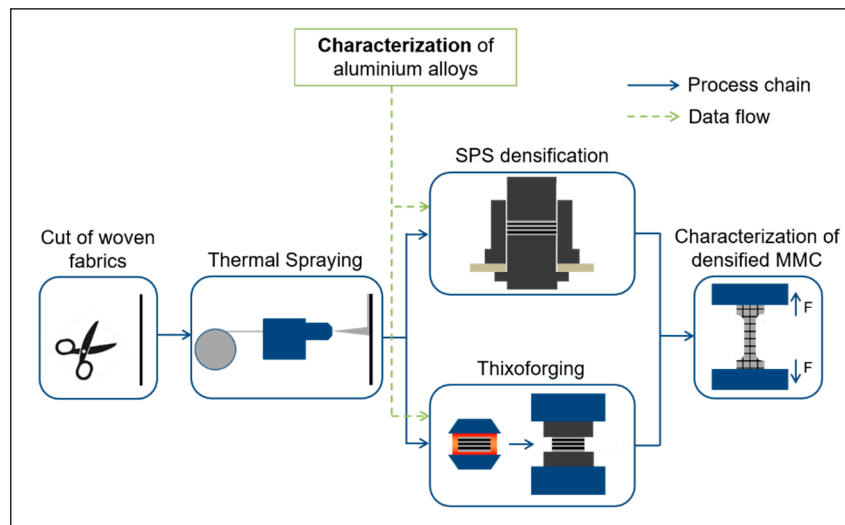


Figure 1. MMC manufacturing process chain.

MMC prepregs consisting of metallized carbon fiber fabrics were manufactured by means of twin wire arc spraying. This spraying technique consists of the continuous mechanical feeding of two metallic wires with the same chemical composition, parallel and with equal speed, into a spray gun. As the wires are electrically charged with opposing polarity, an electric arc is generated between the tips of the wires. The resulting heat melts the metallic feedstock. Molten particles are atomized and accelerated towards the substrate by compressed air flow. A twin wire arc torch Sparc 400 (GTV Verschleißschutz GmbH, Luckenbach, Germany) was used in this study. The torch was mounted on a robot arm, which followed a meander trajectory with a speed of 400 mm/s. The robot arm repeated six times the same trajectory on both sides of the woven fabric with a wire feed speed of 3.9 m/min and an output voltage of 36 V for sustaining the electric arc. After the thermal spraying process, the carbon fiber fabrics are pre-infiltrated by aluminum as shown in Figure 2.

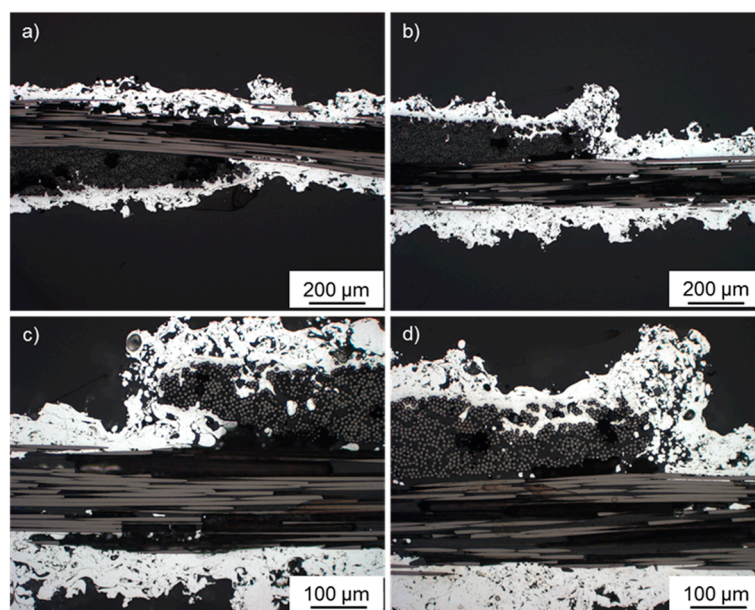


Figure 2. While light microscope images of thermally sprayed fiber prepregs: (a,c) AlSi1MgMn; (b,d) AlSi7Mg.

The resulting coated fabrics were cut in different geometries to fit the die dimensions. In the case of the prepregs for SPS experiments, coated fabrics were cut in circles with a diameter of 49 mm. The SPS graphite die was covered with graphite foil as a release agent layer and eight stacked prepregs were additionally covered with two graphite discs at the top and at the bottom. The fiber prepregs were then consolidated to discs of 49 mm diameter with SPS equipment by FCT Systeme (Rauenstein, Germany). The pulse condition used in this study was 8:2, relating the first number to the time ON and the second to the time OFF (both magnitudes measured in ms). An initial axial pressure of 5 MPa and a preheating of 350 °C were applied to close the gaps between layers and to homogenize the temperature at a value under the liquidus temperature of the alloy. According to the published literature, this value of preheating temperature does not lead to aluminum carbide formation at the fiber/matrix interface [6]. Finally, temperature and pressure were raised to their target values. Three different densification temperatures of the semi-solid temperature range were chosen for every alloy. Furthermore, two different axial pressures—7.5 and 10 MPa—for each densification temperature were investigated. Depending on the alloy, the densification temperature varied between 585 °C and 650 °C. Figure 3 shows exemplarily a densification cycle with a densification temperature of 605 °C and an applied axial pressure of 10 MPa.

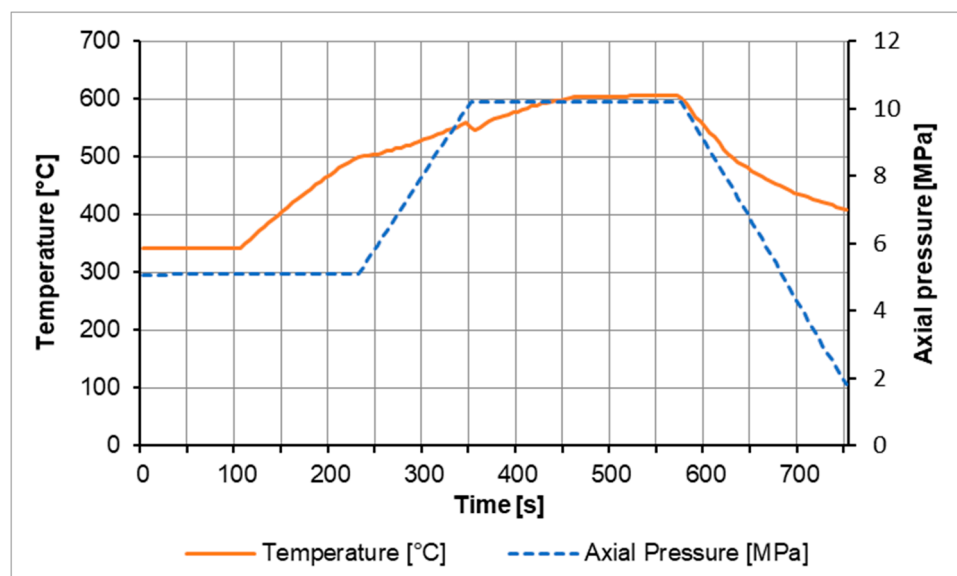


Figure 3. Exemplary thermal and pressure cycles for densification of C_f/Al .

For the thixoforging densification experiments, coated fabrics were cut into rectangular sheets of $120 \times 150 \text{ mm}^2$. Eight prepregs layers were laminated and wrapped with a steel foil of 0.1 mm thickness to avoid loss of liquid fraction of the alloy during densification. In order to enable an easy removal of MMC plates after densification, the interior side of steel foil was impregnated with EKamold[®] boron nitride suspension (3M, Minnesota, USA) as release agent. Prepreg packages were then heated by a propane-powered infrared radiator and transferred to a hydraulic press Type HPS-S 1000 kN by Schuler Hydrap (Plüderhausen, Germany). Target values of pressing force and stroke speed were set to 1000 kN (~67 MPa) and 6 mm/s respectively.

In order to set appropriate densification temperatures for every alloy, melting properties of metal wires were characterized by differential scanning calorimetry (DSC). This method enables the determination of both, the liquidus and solidus temperatures and the temperature dependence of liquid phase content of metals. The DSC tests of this study were conducted with the thermal analyzer DSC822e by Mettler Toledo (Columbus, USA). The DSC tests started with a fast heating rate of 20 K/min from room temperature to 500 °C followed by two different heating rates of 2 and 5 K/min up to 700 °C. The evaluation of the DSC curves to determine the liquid phase fraction as a function of

temperature is based on the integration of the area between curve and baseline according to the standard DIN 51004 [19].

MMC samples of each alloy were consolidated at three different processing temperatures within temperature range of semi-solid state. The consolidation temperatures, which were selected for this study considering results of DSC analysis, are shown in Table 2. There are different reasons for operating under the liquidus line: impeding loss of metal liquid phase during pressing; inhibition of reaction products formation at the interface; reduction of residual stresses; and shrinkage. This manufacturing route, based on semi-solid consolidation of thermally sprayed prepregs, has been previously investigated with alternative consolidation methods, as for instance hydraulic pressing [20–22].

Table 2. Processing temperatures and corresponding liquid phase content for each alloy.

AlSi1MgMn		AlSi5		AlSi7Mg		AlSi10Mg	
Temperature (°C)	Liquid Phase Content (%)						
630	12	595	58	585	66	585	83
640	48	605	65	595	75	590	88
650	100	615	77	605	87	595	94

The MMC samples were afterwards characterized with respect to Young’s modulus by resonance frequency method (IMCE, Belgium) and with respect to flexural strength by static three-point bending tests according to the standard DIN-EN-658-3 “Advanced technical ceramics—Mechanical properties of ceramic composites at room temperature” on a universal testing machine Z100 (Zwick GmbH & Co. KG., Ulm, Germany). The above-mentioned standard was chosen because of the lack of a standard for fiber reinforced metals. SPS densified samples were mechanized by means of waterjet cutting as shown in Figure 4. MMC samples manufactured by thixoforming were cut with a SiC cutting disc. The ratio between sample thickness and supports distances was fixed at a value of 12 for all tests. The setup of the bending test is shown in Figure 4.

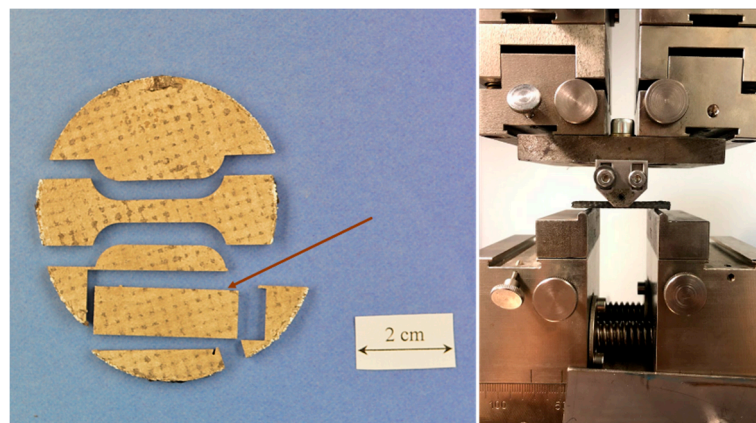


Figure 4. MMC specimens for mechanical characterization and setup of three-point bending test.

The densities of consolidated samples were determined with an analytical balance (Kern ABS, Germany) using the Archimedes principle. The fiber volume fractions were calculated from the results of the density measurements, using the general rule of mixtures of fiber reinforced materials.

$$\rho_c = \rho_m v_m + \rho_f v_f \quad (1)$$

where

ρ_c, ρ_m, ρ_f : densities of composite, matrix and dispersed phase respectively;
 v_m, v_f : volume fraction of matrix and dispersed phase respectively.

3. Results

3.1. Thermal Characterization of Aluminium Alloys

The results of the liquidus and solidus temperatures for each heating rate, according to the evaluation of the DSC curves, are shown in Table 3. With regard to the solidus temperatures, there are deviations of maximum 5 K comparing both heating rates. The differences of liquidus temperatures for both heating rates achieve a maximal value of 8 K. It is a well-known fact that increments of heating rates lead to deviations of DSC curves, which directly influence the values of liquidus and solidus temperatures in this case.

Table 3. Solidus and liquidus temperatures of aluminum alloys according to DSC measurements.

Alloy	Solidus Temperature (°C)		Liquidus Temperature (°C)	
	2 K/min	5 K/min	2 K/min	5 K/min
C _f /AlSi1MgMn	610	605	652	660
C _f /AlSi5	560	560	634	640
C _f /AlSi7Mg	555	550	620	625
C _f /AlSi10Mg	560	560	605	610

Figure 5 shows the temperature dependence of liquid phase content for the investigated samples. The curve slopes are completely different for each alloy. In the case of the casting alloy AlSi10Mg, the inclination of the curve is very pronounced, especially in the range of 10–80% liquid phase content. A similar behavior can be observed for the wrought alloy AlSi1MgMn above 10% liquid phase content. Therefore, prepreps sprayed with these two alloys need to be handled with a very accurate control of processing temperatures in order to reach suitable liquid phase contents for semi-solid shaping. On the other side, the alloys AlSi5 and AlSi7Mg exhibit lower gradients, enabling their processing in semi-solid state.

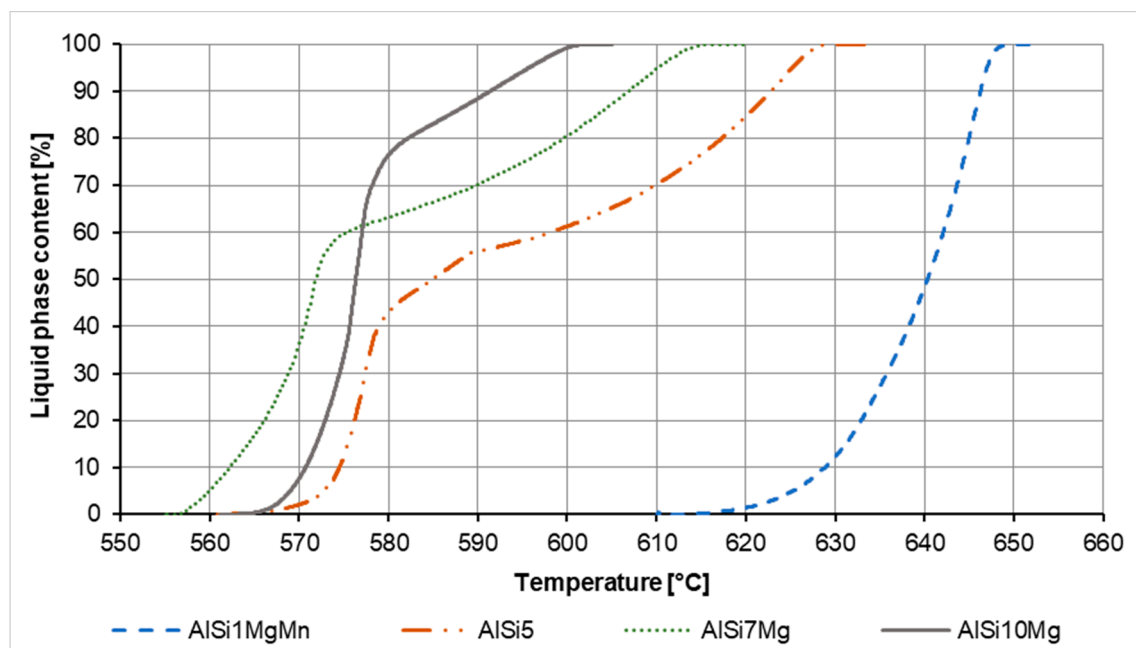


Figure 5. Temperature dependence of liquid phase content of Al alloys according to DSC measurements.

3.2. SPS Consolidation of Samples

In general terms, MMC prepreps from the different aluminum alloys employed in this study were successfully densified in the semi-solid state temperature range of each alloy. Fiber fabrics were

infiltrated by the metallic matrix with nearly no signs of porosity, as observed in Figure 6. The only exception to this behavior are the fiber prepregs sprayed with the cast alloy AlSi10Mg, which already showed a particular melting behavior in the DSC analysis. The extremely high sensitivity of liquid phase content to minor temperature variations (69% increase of liquid phase content between 570 and 580 °C) hampers presumably the consolidation of fabrics metallized with this alloy, leading to the formation of numerous infiltration defects, as observed in Figure 6.

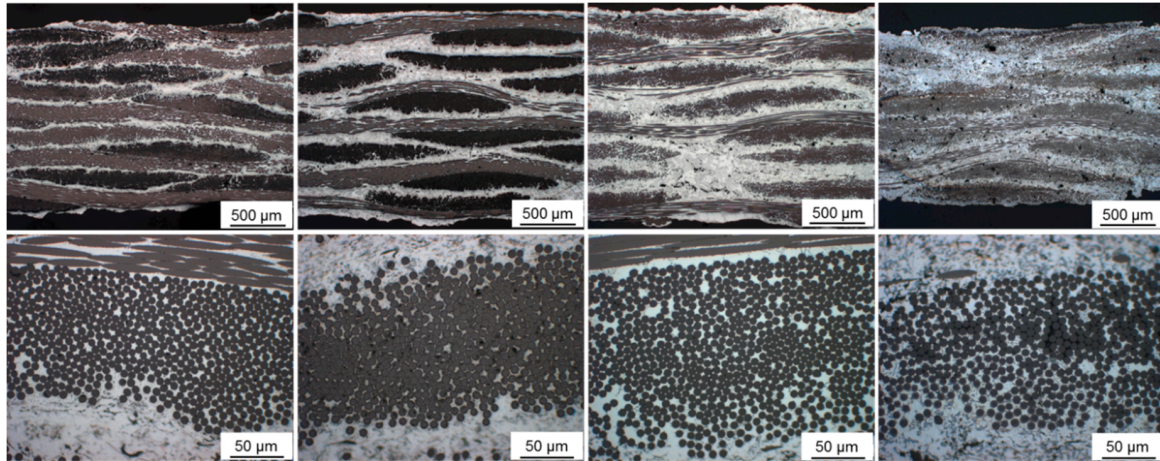


Figure 6. While light microscope images of SPS consolidated MMC samples. From left to right: $C_f/AlSi1MgMn$, $C_f/AlSi5$, $C_f/AlSi7Mg$ and $C_f/AlSi10Mg$.

According to conducted density measurements, fiber volume content of the samples fluctuates between 45% and 54% (see Table 4). An increase of consolidation temperature and axial pressure leads to slightly higher values of fiber volume content. The reason for that is the missing small amount of liquid phase, which is pressed out of the die due to the low viscosity of the metal. Although these values are not atypically elevated for woven reinforced composites, the apparent local fiber volume content around the fiber rovings is too high for an optimal fiber/matrix stress transfer. Distances between single filaments are in some cases inexistent, as shown in the lower images of Figure 6.

Table 4. Fiber volume content estimated from density measurement and rule of mixtures.

Sample	Fiber Volume Content (%)
$C_f/AlSi1MgMn$	50–54
$C_f/AlSi5$	46–49
$C_f/AlSi7Mg$	45–48
$C_f/AlSi10Mg$	48–52

3.3. Mechanical Characterization

The values of bending strength and Young's modulus of SPS consolidated MMC samples for optimal densification parameters are given in Figure 7. For comparison purposes, the mechanical properties of MMC samples from identical prepregs consolidated by thixoforging process with hydraulic press are shown in Figure 8. Although raw materials and prepreg manufacturing process were the same in both cases, the differences of mechanical properties for both groups of samples are remarkable. SPS consolidated samples exhibit much higher stiffness and lower bending strength in comparison with MMC samples manufactured by alternative consolidation methods.

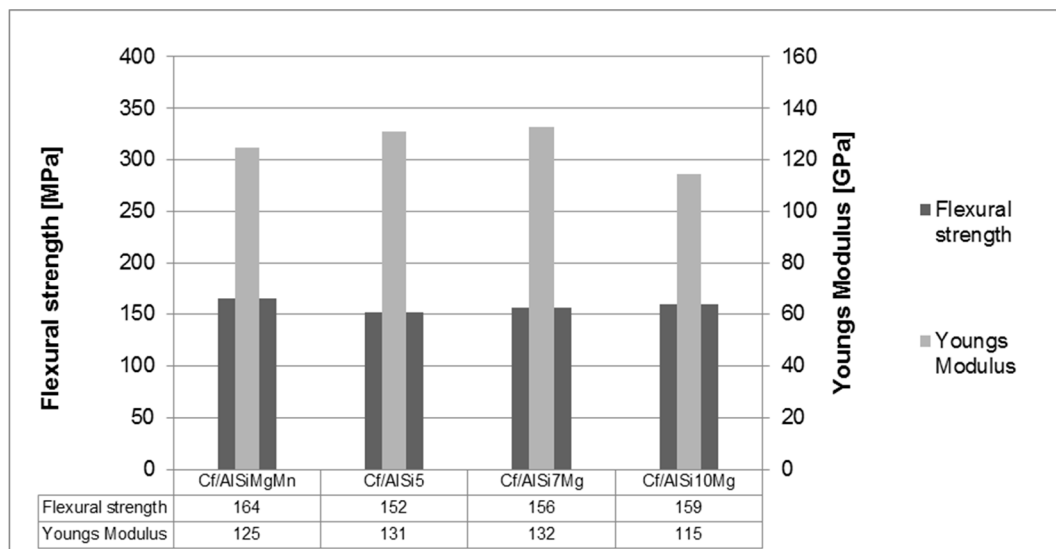


Figure 7. Mechanical properties of SPS consolidated C_f/Al samples for optimum densification parameters.

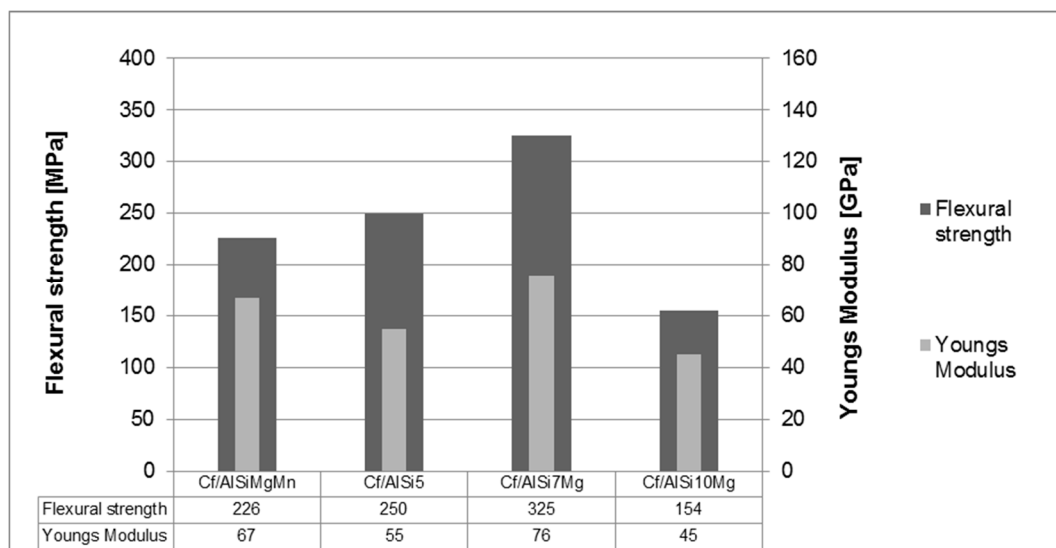


Figure 8. Mechanical properties of C_f/Al samples consolidated by hydraulic pressing for optimum densification parameters.

It is noticeable that, in the case of samples consolidated by SPS, differences of bending strength between each material system are minor. All bending strength values of these samples are higher than 150 MPa and lower than 165 MPa. The reason for his behavior is presumably, that failure mechanisms of SPS consolidated samples are strongly dominated by the elevated interfacial bonding strength. As observed in the failure surface (Figure 9, left image), SPS samples show a brittle behavior without signs of crack deflection, pull-out morphology or fiber debonding. This fact indicates a strong fiber/matrix adhesion, which would be the limiting factor of the composite under flexural stress. This high level of fiber/matrix adhesion could be induced by an uncontrolled growth of interfacial reaction products. Actually, suspicious crystals were found at the fiber surfaces by SEM fractographic analysis of some SPS consolidated MMC samples, as shown for the case of a $C_f/AlSi7$ sample in the central and right images of Figure 9.

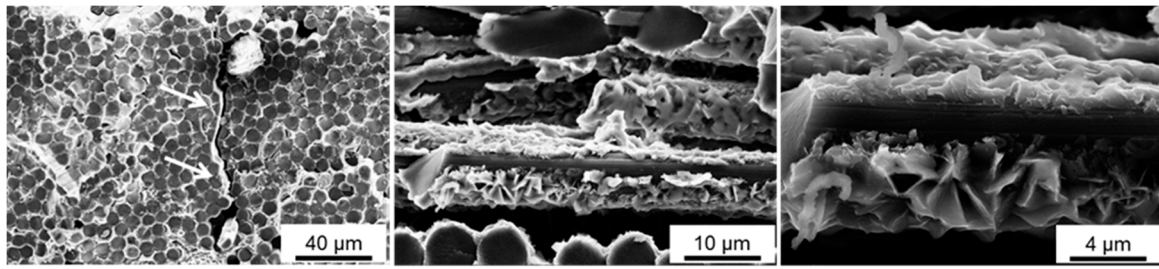


Figure 9. Failure surfaces of SPS-consolidated C_f/Al samples.

3.4. Raman Spectroscopy

This presumed carbide formation on the fiber surface was proven by a Raman spectroscopy measurement. The company TTI GmbH—AViSpectro TGU (Stuttgart, Germany) was commissioned for this purpose. According to the results, aluminum carbide is embedded in the surface of carbon fibers in the form of small crystals. The results of the Raman spectroscopy as well as the microscopic image at one of the points where Al_4C_3 was found are shown in Figure 10.

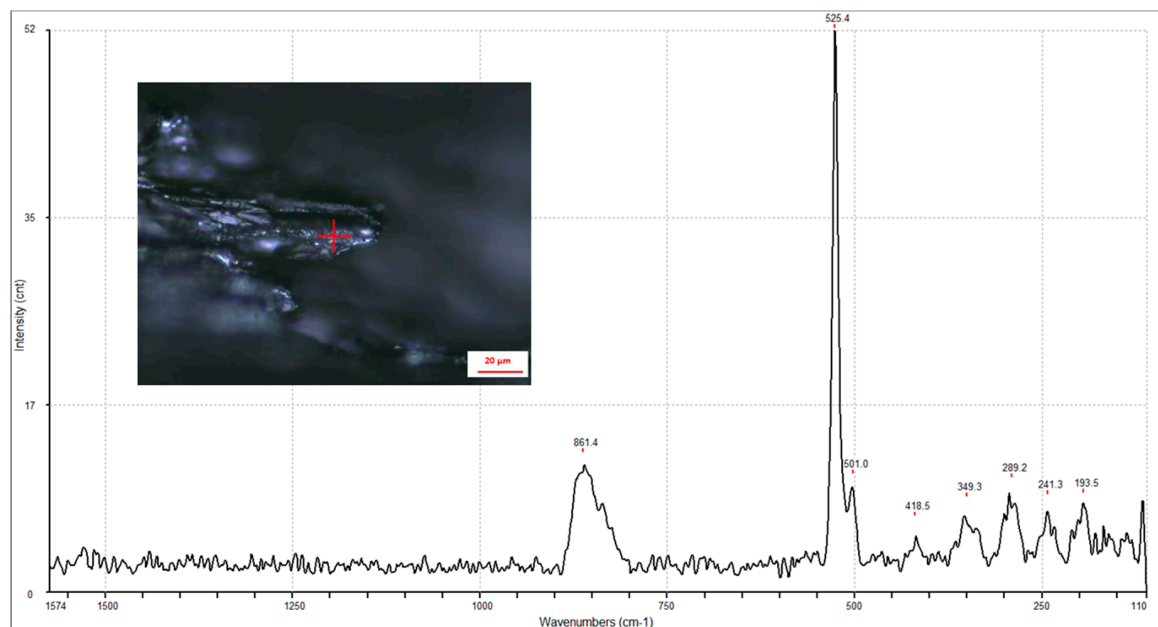


Figure 10. Raman spectrum and microscopic image at the C_f/Al interface.

4. Discussion

The main point to analyze in this chapter is the reason for the notable differences between failure mechanisms and mechanical properties of MMC samples consolidated by SPS and by hydraulic pressing. Considering the morphology of failure surfaces, SPS consolidated samples show no signs of energy dissipation phenomena at the interface. Indeed, aluminum carbide formation at the interface was detected by Raman Spectroscopy only in SPS consolidated samples. These differences of interface properties between both kinds of samples are caused by the different consolidation techniques, as raw materials and prepreg manufacturing parameters were the same for all the samples.

Some recent studies about SPS densification of short carbon fibers and aluminum particles have reported how SPS processing with certain pulse conditions leads to uncontrolled growth of reaction zones at the interface [18]. According to some publications, decreases of the ON:OFF ratio elevates the momentary current intensity, which can increase local processing temperatures due to Joule heating [23,24]. According to Lalet et al., liquid phase was observed at a low ON:OFF ratio, although

having set the processing temperature to 500 °C. This indicates a local temperature increase above the melting point of aluminum (660 °C) during SPS densification of short fiber reinforced aluminum [18]. Following the argumentation of the authors, the Al₂O₃ passivation layer of the Al particles, which were used as raw materials in the mentioned study, might be broken by internal stresses derived from melting-expansion iterations during SPS heating process. An analogy between passivation layers of Al particles of mentioned study and thermal sprayed Al layers of the present study could explain observed results. Although heated below the liquidus temperature, there could be local temperature increases during the SPS process, thus promoting the formation of Al₄C₃.

Regarding the brittle failure mechanisms of SPS consolidated samples, another argument could explain this behavior. The constraint of metallic layers surrounded by reinforcing ceramic phases has been identified in a previous study as a negative-impact factor for toughness of metal matrix composites [25]. Suboptimal filament distribution in the MMC samples of this study, with fibers stacking together in large areas, may impair toughness of the whole composite. An increase of aluminum thickness between filaments would lead to a toughness enhancement.

5. Conclusions

The suitability of SPS technique for production of continuous carbon fiber reinforced aluminum was analyzed and proven for the first time in this work. MMC samples were consolidated with remarkable infiltration results. The stable process management of modern SPS equipment enables an accurate control of main densification parameters: temperature and pressure. This parameter accuracy is required to optimize the shear thinning rheological behavior of aluminum alloys at semi-solid temperatures.

According to the mechanical characterization of the samples, stiffness values in the order of 115–135 GPa were achieved. Considering the low density of this material system, values of specific stiffness double those of standard Al-alloys, like EN AW 6082. However, SPS consolidated composites exhibited reduced damage tolerance and suboptimal interface properties. This aspect should be improved in future studies.

Author Contributions: Conceptualization, M.J., F.K., and R.G.; Methodology, M.J.; Formal analysis, M.J. and F.K.; Investigation, M.J. and F.K.; Resources, R.G.; Data curation, M.J.; Writing—original draft preparation, M.J.; Writing—review and editing, F.K. and F.O.; Visualization, M.J. and F.O.; Supervision, R.G. and F.K.; Project administration, R.G. and F.K.; Funding acquisition, R.G. All authors have read and agreed to the published version of the manuscript.

Funding: This research received no external funding.

Conflicts of Interest: The authors declare no conflict of interest.

References

1. Kainer, K.U. (Ed.) Basics of Metal Matrix Composites. In *Metal matrix composites: Custom-made Materials for Automotive and Aerospace Engineering*; Wiley-VCH: Weinheim, Germany, 2006; pp. 1–54, ISBN 9783527313600.
2. Evans, A.; San Marchi, C.; Mortensen, A. *Metal Matrix Composites in Industry: An Introduction and a Survey*; Kluwer Academic Publishers: Dordrecht, The Netherlands, 2003; ISBN 1402075219.
3. Li, S.-H.; Chao, C.-G. Effects of carbon fiber/Al interface on mechanical properties of carbon-fiber-reinforced aluminum-matrix composites. *Met. Mater. Trans. A* **2004**, *35*, 2153–2160. [[CrossRef](#)]
4. Vidal-Sétif, M.H.; Lancin, M.; Marhic, C.; Valle, R.; Raviart, J.-L.; Daux, J.-C.; Rabinovitch, M. On the role of brittle interfacial phases on the mechanical properties of carbon fibre reinforced Al-based matrix composites. *Mater. Sci. Eng. A* **1999**, *272*, 321–333. [[CrossRef](#)]
5. Wang, J.; Hong, T.; Li, G.; Li, P. A combined process of coating and hybridizing for the fabrication of carbon fiber reinforced aluminum matrix composites. *Compos. Part A: Appl. Sci. Manuf.* **1997**, *28*, 943–948. [[CrossRef](#)]
6. Baker, S.J.; Bonfield, W. Fracture of aluminium-coated carbon fibres. *J. Mater. Sci.* **1978**, *13*, 1329–1334. [[CrossRef](#)]

7. Baker, A.A. Carbon fibre reinforced metals—A review of the current technology. *Mater. Sci. Eng.* **1975**, *17*, 177–208. [[CrossRef](#)]
8. Wielage, B.; Dorner, A. Veränderung des elektrochemischen Korrosionsverhaltens und der mechanischen Eigenschaften von C/Al-Verbunden durch Faserbeschichtungen aus SiC und pyrolytischem Kohlenstoff. *Materialwissenschaft und Werkstofftechnik* **1999**, *30*, 283–290. [[CrossRef](#)]
9. Popovska, N.; Gerhard, H.; Wurm, D.; Poscher, S.; Emig, G.; Singer, R. Chemical vapor deposition of titanium nitride on carbon fibres as a protective layer in metal matrix composites. *Mater. Des.* **1997**, *18*, 239–242. [[CrossRef](#)]
10. Aggour, L.; Fitzer, E.; Heym, M.; Ignatowitz, E. Thin coatings on carbon fibers as diffusion barriers and wetting agents in Al composites. *Thin Solid Films* **1977**, *40*, 97–105. [[CrossRef](#)]
11. Suzuki, T.; Umehara, H. Pitch-based carbon fiber microstructure and texture and compatibility with aluminum coated using chemical vapor deposition. *Carbon* **1999**, *37*, 47–59. [[CrossRef](#)]
12. Bakshi, S.R.; Keshri, A.; Singh, V.; Seal, S.; Agarwal, A. Interface in carbon nanotube reinforced aluminum silicon composites: Thermodynamic analysis and experimental verification. *J. Alloys Compd.* **2009**, *481*, 207–213. [[CrossRef](#)]
13. Portnoi, K.I.; Zabolotskii, A.A.; Timofeeva, N.I. Effect of matrix composition on the reactions of the components of C/Al composite materials. *Met. Sci. Heat Treat.* **1980**, *22*, 813–815. [[CrossRef](#)]
14. Sadeghian, Z.; Lotfi, B.; Enayati, M.H.; Beiss, P. Microstructural and mechanical evaluation of Al–TiB₂ nanostructured composite fabricated by mechanical alloying. *J. Alloys Compd.* **2011**, *509*, 7758–7763. [[CrossRef](#)]
15. Bathula, S.; Anandani, R.; Dhar, A.; Srivastava, A. Synthesis and Characterization of Al-Alloy/SiCp Nanocomposites Employing High Energy Ball Milling and Spark Plasma Sintering. *Adv. Mater. Res.* **2011**, *410*, 224–227. [[CrossRef](#)]
16. Bakshi, S.R.; Lahiri, D.; Agarwal, A. Carbon nanotube reinforced metal matrix composites—A review. *Int. Mater. Rev.* **2010**, *55*, 41–64. [[CrossRef](#)]
17. Lalet, G.; Kurita, H.; Miyazaki, T.; Kawasaki, A.; Silvain, J.-F. Thermomechanical stability of a carbon fiber-reinforced aluminum matrix composite fabricated by spark plasma sintering in various pulse conditions. *Mater. Lett.* **2014**, *130*, 32–35. [[CrossRef](#)]
18. Lalet, G.; Kurita, H.; Miyazaki, T.; Kawasaki, A.; Silvain, J.-F. Microstructure of a carbon fiber-reinforced aluminum matrix composite fabricated by spark plasma sintering in various pulse conditions. *J. Mater. Sci.* **2014**, *49*, 3268–3275. [[CrossRef](#)]
19. Deutsches Institut für Normung (DIN). *Thermal Analysis—Determination of Melting Temperatures of Crystalline Materials by Differential Thermal Analysis*; DIN 51004; German Institute for Standardisation (Deutsches Institut für Normung): Berlin, Germany, 1994.
20. Wenzelburger, M.; Silber, M.; Gadow, R. Manufacturing of Light Metal Matrix Composites by Combined Thermal Spray and Semisolid Forming Process—Summary of the Current State of Technology. *Key Eng. Mater.* **2010**, *425*, 217–244. [[CrossRef](#)]
21. Silber, M.; Wenzelburger, M.; Gadow, R. New manufacturing process for thermally sprayed prepregs with local UD fiber reinforcement for semi solid forming of light metal MMC. *Int. J. Mater. Form.* **2009**, *2*, 745–748. [[CrossRef](#)]
22. Wenzelburger, M.; Nieves Alsina, M.; von Niessen, K.; Gadow, R. Thermal Spray Manufacturing of Semi-Finished Parts for Thixoforming of Fiber and Particle Reinforced Metal Matrix Composites. *Solid State Phenom.* **2006**, *116*, 375–378. [[CrossRef](#)]
23. Cincotti, A.; Locci, A.M.; Orrù, R.; Cao, G. Modeling of SPS apparatus: Temperature, current and strain distribution with no powders. *AIChE J.* **2007**, *53*, 703–719. [[CrossRef](#)]
24. Chen, W.; Anselmi-Tamburini, U.; Garay, J.E.; Groza, J.R.; Munir, Z.A. Fundamental investigations on the spark plasma sintering/synthesis process. *Mater. Sci. Eng. A* **2005**, *394*, 132–138. [[CrossRef](#)]
25. Cutler, R.A.; Virkar, A.V. The effect of binder thickness and residual stresses on the fracture toughness of cemented carbides. *J. Mater. Sci.* **1985**, *20*, 3557–3573. [[CrossRef](#)]

